Efficient production of the nuclear isomer ^{93m}Mo with laser-accelerated proton beam and its astrophysical implication on ^{92}Mo production

Wenru Fan,[1,*] Wei Qi,[2,*] Jingli Zhang,[1] Zongwei Cao,[1] Haoyang Lan,[3] Xinxiang Li,[1] Yi Xu,[4] Yuqiu Gu,[2] Zhigang Deng,[2] Zhimeng Zhang,[2] Changxiang Tan,[1] Wen Luo,[1,†] Yun Yuan,[1,‡] and Weimin Zhou[2,§]

[1]*School of Nuclear Science and Technology, University of South China, 421001 Hengyang, China*

[2]*Science and Technology on Plasma Physics Laboratory, Laser Fusion Research Center, China Academy of Engineering Physics, 621900 Mianyang, China*

[3]*State Key Laboratory of Nuclear Physics and Technology, and Key Laboratory of HEDP of the Ministry of Education, CAPT, Peking University, 100871 Beijing, China*

[4]*Extreme Light Infrastructure—Nuclear Physics (ELI-NP), Horia Hulubei National Institute for R&D in Physics and Nuclear Engineering (IFIN-HH), 30 Reactorului Str., 077125 Buchurest-Magurele, Romania*

(Received 2 May 2023; accepted 29 September 2023; published 6 November 2023)

Nuclear isomers play a key role in the creation of the elements in the universe and potentially have significant applications related to the controlled release of nuclear energy on demand. Particularly, ^{93m}Mo is a good candidate for studying the depletion of nuclear isomers via nuclear excitation by electron capture. Therefore, it is necessary to explore the efficient approach of ^{93m}Mo production. In this paper, we experimentally demonstrate an efficient production of ^{93m}Mo via ^{93}Nb(p,n) reaction induced by an intense laser pulse. Employing the picosecond-duration, 100 J laser pulse, the ^{93m}Mo isomer at 2425 keV ($21/2^+$, $T_{1/2} = 6.85$ h) is generated with a high yield of 1.8×10^6 particles/shot. The resulting peak production efficiency reaches 10^{17} particles/s, which is at least five orders of magnitude higher than that obtained using the classical accelerator. The impacts of the production and destruction of ^{93m}Mo to the astrophysical p-nuclide ^{92}Mo are studied. It is found that the ^{93}Nb(p,n) ^{93m}Mo reaction is an important production path of ^{93m}Mo, which could further influence the production of ^{92}Mo. In addition, a direct measurement of the (p,n) reaction rate is proposed using the laser-induced proton beam of which the energies follow the Maxwell-Boltzmann distribution well. It is believed that the laser-induced proton beam opens an avenue for the production of nuclear isomers with high peak efficiency used for the studies of p-nuclei nucleosynthesis.

DOI: 10.1103/PhysRevResearch.5.043120

I. INTRODUCTION

Nuclear isomers are relatively long-lived metastable excited states, with the half-lives ranging from nanoseconds to years. The long half-lives of the isomers provide a unique opportunity to explore nucleosynthesis in extreme astrophysical environments [1,2]. In such a nucleosynthesis calculation, the accurate nuclear reaction rates are expected, especially for some reactions that can dramatically influence the path of nucleosynthesis [3,4]. Nuclear isomers also have a broad range of potential applications including nuclear batteries [5–7], medical isotopes [8–10], nuclear clocks [11,12], and nuclear γ-ray lasers [13]. For example, the nuclear batteries composed of nuclear isomers have a much higher energy density than chemical batteries and hence are considered good energy sources for deep space exploration.

Recently, the manipulation of the nuclear isomer ^{93m}Mo has gained lots of attention. Here, ^{93m}Mo has a $(21/2)^+$ isomer at 2425 keV with a half-life of 6.85 h and a $(17/2)^+$ intermediate state that lies 4.85 keV higher at 2430 keV with a half-life of 3.5 ns. Such an isomeric property is attractive in nuclear medical applications [14] and studies of nuclear isomer depletion via nuclear excitation by electron capture (NEEC) [15–18]. Polasik *et al.* [16] provided experimental evidence of ^{93m}Mo isomer depletion caused by NEEC. However, the reported depletion probability is a few orders of magnitude higher than the theoretical expectation [19], and such isomer depletion was not confirmed by another dedicated experiment [20]. To investigate the depletion of the nuclear isomer ^{93m}Mo, it is necessary to efficiently produce them.

In nucleosynthesis studies, a particularly challenging question is the creation of the so-called 35 p-nuclei between ^{74}Se and ^{196}Hg, which can be produced under the explosive conditions in a sequence of photodisintegration reactions [21]. Among these p-nuclei, ^{92}Mo (neutron number $N = 50$) is a neutron-magic p-nuclide and exhibits larger abundances than the neighboring p-nuclei. Figure 1 shows the production of a ^{92}Mo isotope by different photodisintegration paths. These paths include the ^{93}Mo(γ,n), ^{93}Tc(γ,p), and ^{96}Ru(γ,α)

*These authors contributed equally to this paper.
†wen.luo@usc.edu.cn
‡yuanyun_usc@qq.com
§zhouwm@caep.cn

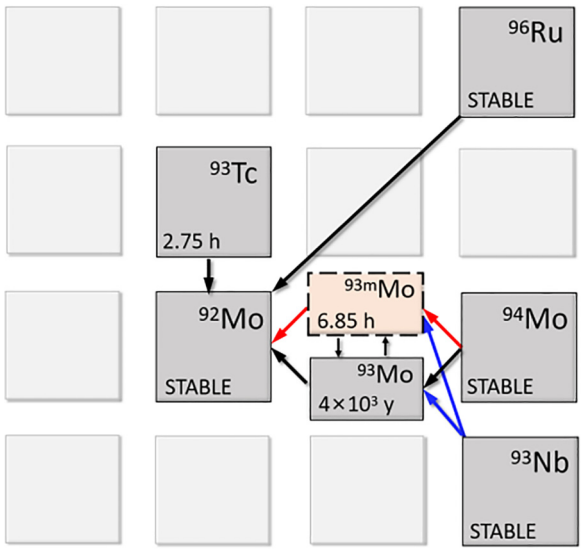

FIG. 1. An excerpt of the chart of nuclei depicting the production of ^{92}Mo via photodisintegration reactions. The red lines indicate the reaction flow through ^{93m}Mo that may affect the abundance of ^{92}Mo in extreme astrophysical environments. The blue lines show the production of ^{93}Mo in the ground state and isomeric state via proton-induced reactions.

reactions. Recently, authors of a nucleosynthesis sensitivity study showed that the ^{92}Mo isotope is mainly produced by photodisintegration of ^{93}Mo [22]. However, the production of ^{92}Mo in stars is a puzzle in nuclear astrophysics since the present nucleosynthesis models underestimate this *p*-nuclide by several orders of magnitude. When calculating the astrophysical reaction rates, the involved nuclei are typically assumed to be in the ground state or the excited levels following the thermal equilibrium probability distribution [23]. However, such an assumption may not be valid for the actual astrophysical circumstances. Some nuclear isomers, which play an essential role in nucleosynthesis, should be treated as individual species, i.e., the astromers [2]. Here, ^{93m}Mo is one of the astromers which may affect the abundance of ^{92}Mo via the subsequent (γ,*n*) reaction. Therefore, it is worth considering whether the ^{93m}Mo - ^{92}Mo reaction flow is involved in the production of the missing *p*-nuclide ^{92}Mo.

The production of ^{93m}Mo has been realized by using radiofrequency accelerators [24–27]. In a recent experiment showing the evidence of NEEC with a reported beam intensity of $\sim 6 \times 10^8$ ions/s, the total production rate of ^{93m}Mo is estimated to be $\sim$9.3 kHz [28]. It should be noted that such a production rate is not efficient for the following isomer depletion, considering the insufficient NEEC rate. With the rapid development of ultraintense and ultrashort laser technology [29], laser intensity focused on the target can exceed 10^{22} W/cm^2. High-intensity lasers can produce energetic particle beams with large charges for many pioneering applications [30–33]. It was theoretically investigated that the laser-wakefield accelerated electrons could be used to produce a series of nuclear isomers from the photonuclear reactions on ^{197}Au, ^{180}Hf, ^{159}Tb, ^{115}In, ^{103}Rh, and ^{90}Zr [34]. The ^{83m}Kr isomer was populated successfully by the Coulomb collision of ions with quivering electrons with a peak efficiency of 2.34×10^{15} particles/s, which is five orders of magnitude higher than the one achieved by classical accelerator [35].

In this paper, we experimentally demonstrate the efficient production of ^{93m}Mo by laser-accelerated proton beam, through ^{93}Nb(p, n) reaction. For a single picosecond-duration, 100 J laser pulse, the ^{93m}Mo isomer at 2425 keV ($21/2^+$, $T_{1/2} = 6.85$ h) can be generated with a high yield of 1.8×10^6 particles/shot, and the resulting peak production efficiency exceeds 10^{17} particles/s. The effect of nuclear reaction flow on the population of ^{93m}Mo is studied. Here, ^{93m}Mo involved the photodisintegration reactions, leading to the production of ^{92}Mo, which is one of the most debated *p*-nuclei, which is then discussed. Finally, the astrophysical reaction rates of ^{93}Nb(p, n) ^{93m}Mo at *p*-process temperatures are directly deduced from the spectra of the laser-accelerated proton beam that matches well with the Maxwell-Boltzmann (M-B) distribution at high energies [36].

II. METHODS

A. Experiment

The laser-induced proton generation and the following ^{93m}Mo population experiments were performed at the XingGuangIII laser facility at the Laser Fusion Research Center in Mianyang. The experimental setup and target arrangement are schematically shown in Figs. 2(a) and 2(c). In the first stage of our experiments, a laser pulse of 840 fs (full width at half maximum), with 116 J of energy is focused by an off-axis parabolic mirror onto a thin Cu foil with thickness varying from 7 to 15 μm, which then generates a high-energy proton beam that enables triggering the ^{93}Nb(p, n) ^{93m}Mo reaction. A radiochromic film (RCF) stack is used to diagnose the angular distribution of the proton beam and a Thomson parabolas spectrometer (TPS) to detect the energy spectrum of protons passing through a hole in the center of the RCF stack. In the second stage, the RCF stack and the TPS are removed, and the laser-accelerated proton beam directly impinges the Nb target, which has a natural abundance of 99.9% and a thickness of 1 mm and is placed $\sim$14 mm downstream from the Cu foil. The ^{93}Mo isotope in the ground and excited states are then produced through (p, n) reactions. After irradiation, the Nb target is taken out from the target chamber of the XingGuangIII laser facility. Offline detection of the activated Nb target is then performed with a ^{60}Co-calibrated high-purity germanium (HPGe) detector.

B. Simulation

To model the interaction of the laser-accelerated proton beam with the Nb target, we employed the GEANT4-GENBOD toolkit [37,38], in which the photonuclear cross-section data from theoretically computed or experimental databases are considered as the inputs. This toolkit has been used for studies of medical isotope production using intense laser-plasma electron sources [32]. The experimental spectral and angular distributions of the proton beam and the simulated cross-section for the ^{93}Nb(p, n) reaction are considered in the GEANT4 simulations. The Nb target used for proton irradiation has $\sim$100% natural abundance. The target geometry and installation follow the experimental setup.

The calculations of the cross-sections and the astrophysical reaction rates were performed with TALYS 1.9 [39]. The

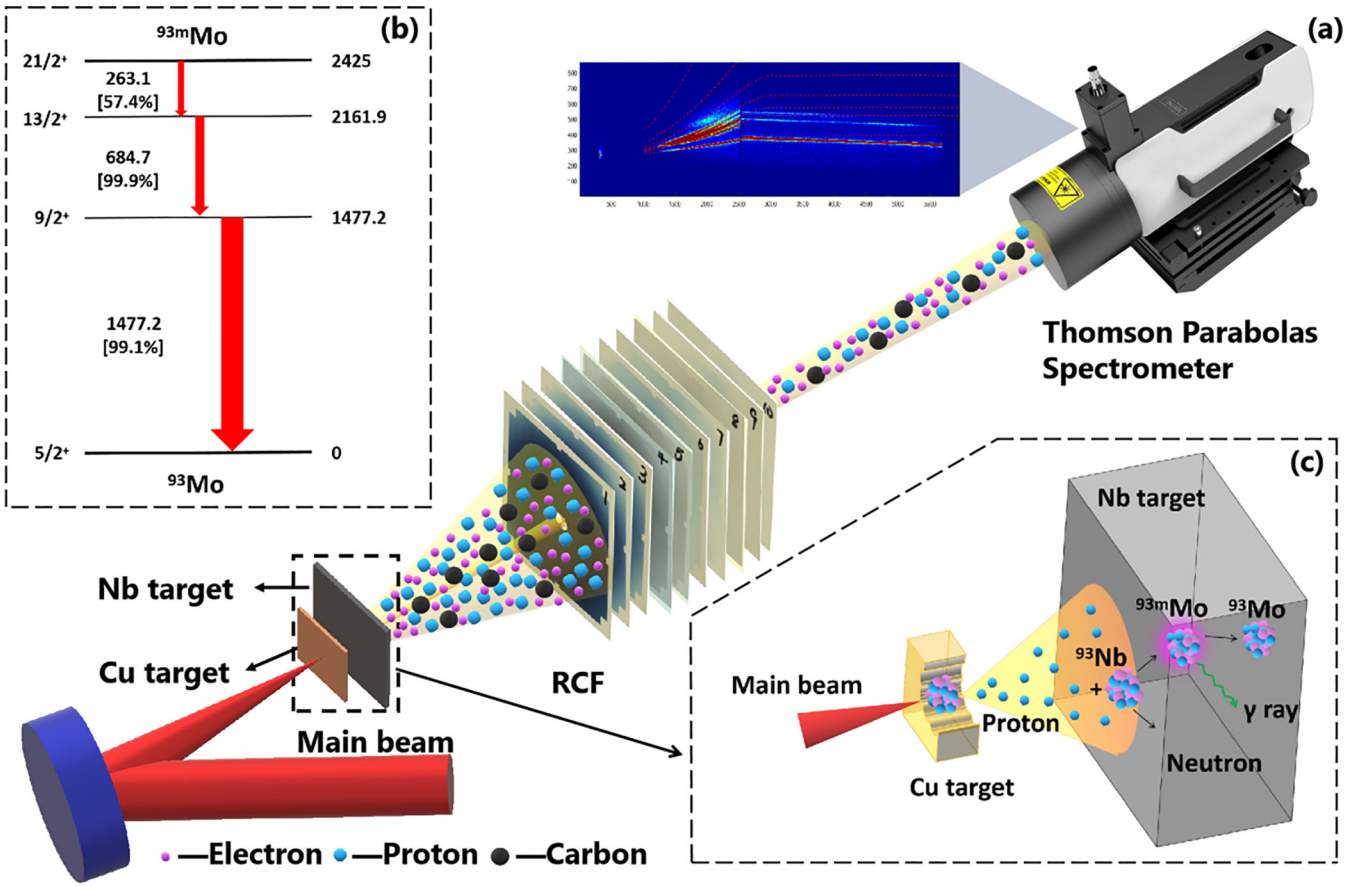

FIG. 2. (a) Schematic diagram of the experimental setup for nuclear isomer ^{93m}Mo production at the XingGuangIII laser facility (not to scale). (b) Partial level scheme (not to scale) for the ^{93m}Mo nucleus ($Z = 42$). The right side of the panel gives the level energies (in keV) and half-lives, and the left side gives the angular momenta and parities. (c) Schematic diagram of the target arrangement for the laser proton acceleration and the following ^{93m}Mo production.

nuclear structure ingredients used for the TALYS computations are explicitly presented in Ref. [40].

III. RESULTS

A. Laser-accelerated proton beam

Recently, laser-accelerated proton beams within the millielectronvolt range have drawn considerable interest because of their potential applications in experimental astrophysics [41], medical isotope production [42,43], and inertial confinement fusion [44]. In our experiments, the energetic protons used for the ^{93m}Mo population are mainly produced through the target normal sheath acceleration (TNSA) [45]. The proton beam generation is optimized by varying the thickness of Cu foil. For three thicknesses of 7, 10, and 15 μm, the energy spectra and angular distributions of the proton beam are

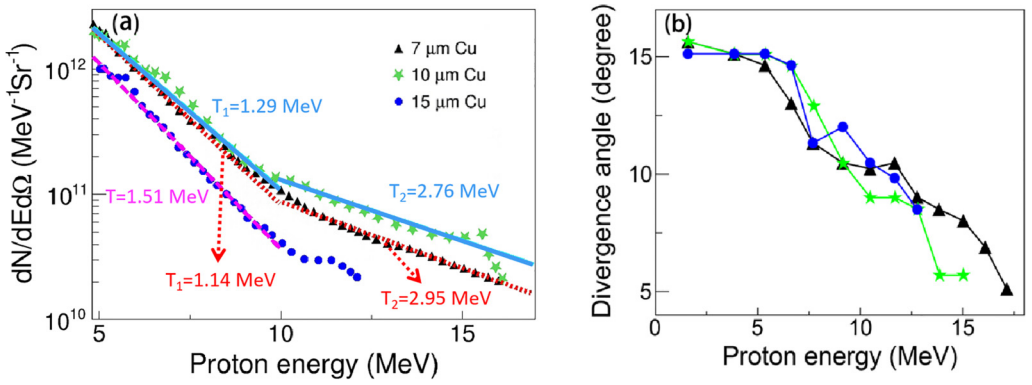

FIG. 3. (a) The energy spectra and (b) angular patterns of protons obtained by irradiating Cu foils with picosecond-duration, 100 J laser pulses. These temperatures are fitted to be $T_1 = 1.14$ MeV, $T_2 = 2.95$ MeV for the 7 μm Cu foil, and $T_1 = 1.29$ MeV, $T_2 = 2.76$ MeV for the 10 μm Cu foil. However, a single M-B distribution with $T = 1.51$ MeV appears in the case of the 15 μm Cu foil.

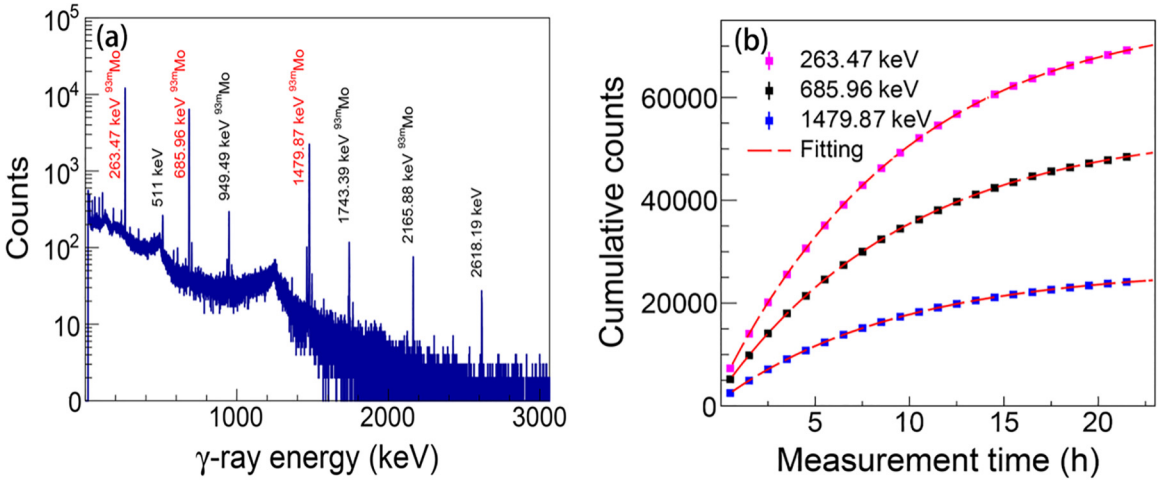

FIG. 4. (a) Exemplary high-purity germanium (HPGe) γ-ray spectrum for Nb target with a measurement time of 22 h. (b) Peak counts accumulated for three characteristic γ-ray lines at the energies of 263.47, 685.96, and 1479.87 keV.

obtained and displayed in Fig. 3. It is shown that the proton energy $E_p < 10$ MeV, and the energy spectra fit well with the M-B distribution [46]:

$$f(E) = \frac{E}{(kT)^2}\exp\left(-\frac{E}{kT}\right), \tag{1}$$

where k is the Boltzmann constant, and T is the proton temperature. In the 7- and 10-μm-thick cases, the measured proton spectra indicate two-temperature M-B distributions. These temperatures are fitted to be $T_1 = 1.14$ MeV, $T_2 = 2.95$ MeV for the 7 μm Cu foil and $T_1 = 1.29$ MeV, $T_2 = 2.76$ MeV for the 10 μm Cu foil. However, a single M-B distribution with $T = 1.51$ MeV appears in the case of the 15 μm Cu foil. The total charges of protons with $E_p > 4$ MeV, which is slightly higher than the reaction threshold of ^{93}Nb(p, n) ^{93m}Mo ($E_{\text{th}} = 3.7$ MeV), are obtained to be 808, 816, and 403 nC for 7-, 10-, and 15-μm-thick Cu foil, respectively. Figure 3(b) demonstrates a strong correlation between proton energy and angular divergence, which decreases with the increasing proton energy. The maximum divergence angle is ∼15°, which is independent of the thickness of Cu foil in our case. Considering the proton charge and temperature, the 10-μm-thick Cu foils were selected for the subsequent ^{93m}Mo population experiments.

B. ^{93m}Mo isomer production

The Nb target used for the ^{93m}Mo production was placed inside the vacuum chamber. After irradiation, it took ∼30 min to reduce the vacuum level of the chamber before the target was removed for offline detection. The produced ^{93m}Mo isomers have a half-life of 6.85 h and three principal characteristic emissions at energies of 263.05, 684.69, and 1477.14 keV. Their respective branching intensity is $I_\gamma = 57.4$, 99.9, and 99.1%, see Fig. 2(b). These characteristic γ rays emitted from the Nb targets were detected successfully with the HPGe detector, as shown in Fig. 4(a). During the offline detection, the Nb target was positioned 1.4 cm away from the endcap of the detector, which weakens the sum-peak effect induced by the simultaneous detection of two or more characteristic γ rays, as discussed later. Figure 4(b) displays the cumulative peak counts of the three characteristic γ-ray lines as a function of the measurement time. The fitting function follows the typical formula for nuclear decay:

$$N_{\text{det}} = N_0\left[1 - \exp\left(-\frac{\ln 2}{T_{1/2}}t\right)\right], \tag{2}$$

where N_{det} is the peak count accumulated at time instant t, and N_0 is the total peak count when all ^{93m}Mo isomers finish their decays. According to Eq. (2), the half-lives of the three γ-ray lines at the energies of 263.05, 684.69, and 1477.14 keV are determined to be 6.89 ± 0.06, 6.95 ± 0.10, and 6.81 ± 0.10h, respectively. These results are in good agreement with the theoretical value of ^{93m}Mo ($T_{1/2} = 6.85$ h) provided by the National Nuclear Data Center database [47].

As mentioned above, the laser-accelerated proton beam follows the M-B distribution. Using Eq. (1), the production yield of the ^{93m}Mo isomers can be written as

$$Y = \frac{nd}{(kT)^2}N_p\int_0^\infty \sigma(E)E\exp\left(-\frac{E}{kT}\right)dE, \tag{3}$$

where n denotes the number density of the target nuclei, d represents the thickness of the Nb target, N_p is the total number of energetic protons irradiating the Nb target, and $\sigma(E)$ represents the cross-section for ^{93m}Mo through proton-induced reaction. For ^{93}Nb(p, n) ^{93m}Mo reaction, Fig. 5 shows the experimental cross-sections and the theoretical data calculated from TALYS software [39]. The calculated results exhibit satisfactory agreement with the available experimental ones for $E_p < 16$ MeV. The reaction cross-section peaked at $E_p = 12.5$ MeV, and the maximum cross section is ∼35 mb.

The yield of the ^{93m}Mo isomers produced in the experiment can be obtained by the peak count of characteristic γ rays using

$$Y_{\text{exp}} = \frac{N_{\text{det}}}{PI_\gamma\varepsilon[1 - \exp(-\lambda\, t_m)]\exp(-\lambda\, t_d)}, \tag{4}$$

where t_m is the real measurement time, t_d is the delay (cooling) time between target irradiation and initial detection, λ represents the decay constant of the ^{93m}Mo isomer, and ε represents

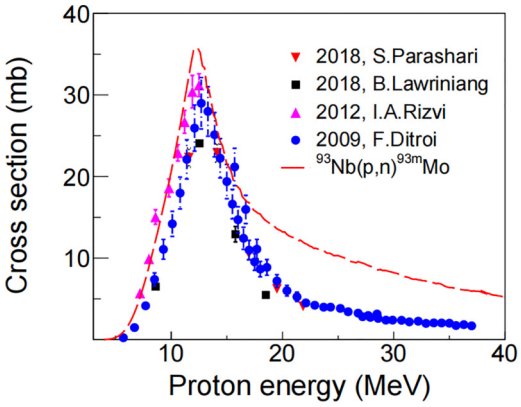

FIG. 5. Cross-section curve of ^{93}Nb(p, n) ^{93m}Mo reaction calculated by TALYS software [39] together with the available experimental data [48–50].

the detection efficiency of the HPGe detector depending on the characteristic γ-ray energy. At $t_m = 22$ h, the $N_{\rm det}$ values for the three characteristic γ rays at 263.05, 684.69, and 1477.14 keV are $(6.92 \pm 0.03) \times 10^4$, $(4.84 \pm 0.03) \times 10^4$, and $(2.43 \pm 0.02) \times 10^4$ per shot, respectively. According to Eq. (4), $Y_{\rm exp}$ is obtained to be $(1.77 \pm 0.01) \times 10^6$, $(1.66 \pm 0.01) \times 10^6$, and $(1.60 \pm 0.01) \times 10^6$ per shot, respectively. Table I summarizes the basic parameters of the three characteristic γ-ray lines and the resulting production yields for ^{93m}Mo isomers. There are evident differences between the production yields obtained by the peak counts of the three characteristic γ rays. Such a discrepancy can be attributed to the sum-peak effect. As illustrated in Fig. 4(a), apart from these primary characteristic γ-ray peaks, three additional high-energy γ rays located at 949.49, 1743.39, and 2165.88 keV are observed. By fitting the curves for their peak counts, their respective half-lives are determined to be 6.89 ± 0.06, 6.95 ± 0.10, and 6.81 ± 0.10h, respectively, which are consistent with the recommended half-life ($T_{1/2} = 6.85$ h) of the ^{93m}Mo isomer within the statistical uncertainty. This indicates that these peaks originate from the radiation decay of the ^{93m}Mo isomer at 2425 keV. For example, the 949.49 keV peak is caused by the sum of two characteristic γ-ray lines at 263.1 and 684.7 keV. Considering the sum-peak effect, the $Y_{\rm exp}$ value is corrected to be $\sim 1.8 \times 10^6$ per shot.

Figure 6(a) depicts the simulated temporal evolution of the ^{93m}Mo isomers for three different thicknesses of Cu foils, as shown in Fig. 3. For the Cu foils of 7 and 10 μm, the production durations of the ^{93m}Mo isomers are estimated to be 65 ps. Accordingly, the peak production efficiencies are evaluated to be 2.77×10^{16} particles/s. The spatial distribution of ^{93m}Mo produced by the ^{93}Nb(p, n) reaction is shown in Fig. 6(b). One can see that the ^{93m}Mo isomers are predominantly generated in the central region of the transverse plane (X-Y plane), and the isomer density decreases with the increasing transversal distance. This is attributed to the fact that the high-energy protons with smaller divergence angles have a greater probability of producing the ^{93m}Mo isomers. Along the longitudinal direction (Z axis), the isomer density decreases because of the limited penetration depth of the proton beam. Note that this trend is beneficial to optimizing the target dimension employed for the isomer production [32].

It is very interesting to investigate the dependence of ^{93m}Mo excitation on the proton temperature. Figures 7(a) and 7(b) show that the ^{93m}Mo yield increases with the increasing proton temperature, whereas the production duration remains almost unchanged. Accordingly, the peak production efficiency of ^{93m}Mo is enhanced with the proton temperature; however, the trend of such enhancement slows down at the relatively high proton temperature, as shown in Fig. 7(b). When the proton temperature becomes >2.25 MeV, the peak excitation efficiency exceeds 10^{17} particle/s. Such efficient isomer excitation may be helpful to explore the NEEC and NEET effects since, currently, the detection of these effects is very challenging due to the extremely low isomer depletion probability and significant background signals [51].

C. Astrophysical implication on ^{92}Mo production

As aforementioned, the underestimation of the abundance of the p-nuclide ^{92}Mo in stars is a pending problem in nuclear astrophysics, which may result from the lack of consideration for isomer contributions in nuclear network calculations. The astrophysical reaction rate of (γ,n) can be written by [52]

$$\mathrm{r}_\gamma = \frac{8\pi}{h^3 c^2} \int_0^\infty \frac{E_\gamma^2}{\exp(E_\gamma/KT) - 1} \sigma(E_\gamma) dE_\gamma, \qquad (5)$$

where h is the Planck constant, c is the velocity of light in vacuum, and E_γ is the γ-photon energy. To briefly evaluate the effect of ^{93m}Mo destruction on ^{92}Mo production, the cross-section of the ^{93m}Mo(γ,n) reaction and its astrophysical reaction rate are calculated and then compared with those of ^{96}Ru (γ, α), ^{93}Tc(γ, p), and ^{93}Mo(γ, n) reactions, as shown in Fig. 8. At the p-process temperatures, the cross-section curves of four photodisintegration reactions leading to the ^{92}Mo production are peaked at almost the same proton energy $\sim$16 MeV. The maximum cross-sections for the ^{93m}Mo(γ,n) and ^{93}Mo(γ, n) reactions are higher than those for the ^{96}Ru (γ, α) and ^{93}Tc(γ, p) reactions. Figure 8(b) shows that the astrophysical reaction rate of ^{93m}Mo(γ, n) ^{92}Mo is visibly lower than the ^{93}Tc(γ, p) ^{92}Mo rate since the latter has a significantly lower reaction threshold, but it is still

TABLE I. The basic parameters of three principal characteristic γ-ray lines and the resulting production yield for ^{93m}Mo isomers.

Isomer	E_γ (keV)	I_γ (%)	$E_{\gamma,\rm exp}$ (keV)	$T_{1/2,\rm exp}$ (h)	$N_{\rm det}$ ($\times 10^4$)	$Y_{\rm exp}$ ($\times 10^6$)
^{93m}Mo	263.05	57.4%	263.47 ± 2.62	6.89 ± 0.06	6.92 ± 0.03	1.77 ± 0.01
	684.69	99.9%	685.96 ± 1.65	6.95 ± 0.10	4.84 ± 0.03	1.66 ± 0.01
	1477.14	99.1%	1479.87 ± 4.31	6.81 ± 0.10	2.43 ± 0.02	1.60 ± 0.01

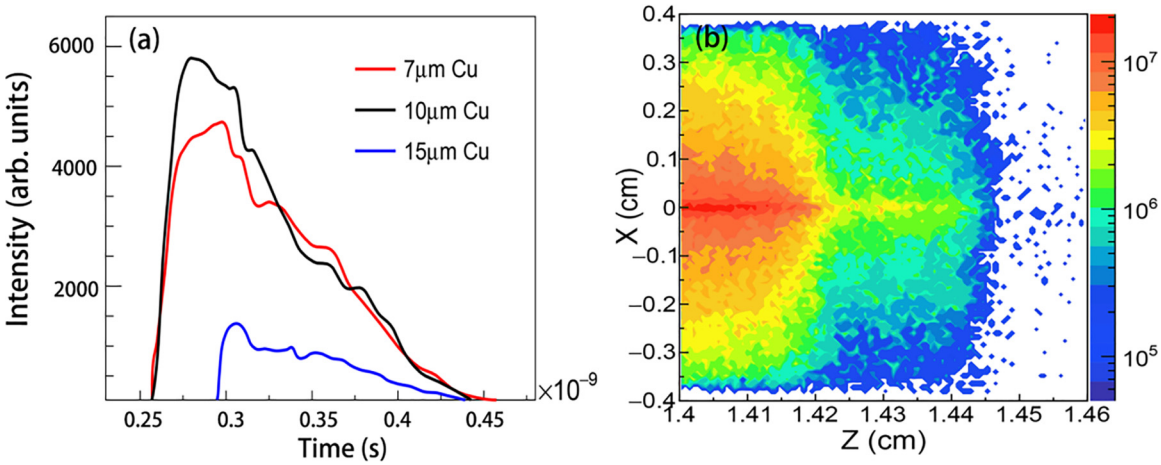

FIG. 6. The simulated (a) temporal and (b) spatial distributions of the ^{93m}Mo isomers produced in the Nb target. The experimental data for the proton beam shown in Fig. 2 are used in the simulations. To expedite the computational process and improve the statistical precision, the simulated cross-section data of the ^{93}Nb(p, n) reaction shown in Fig. 5 are artificially amplified by a factor of 100 in the simulations.

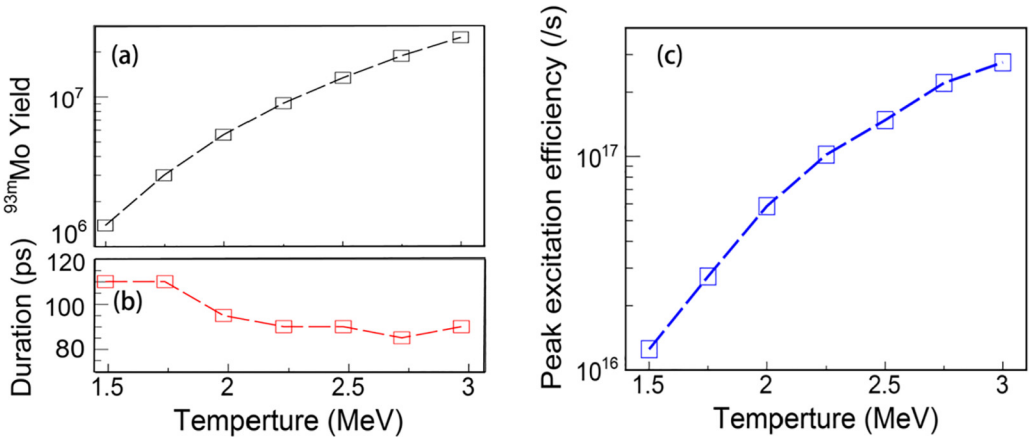

FIG. 7. The ^{93m}Mo (a) yield, (b) duration, and (c) the resulting peak excitation efficiency as a function of proton temperature. The charge of the proton beam used in the simulations is 816 nC.

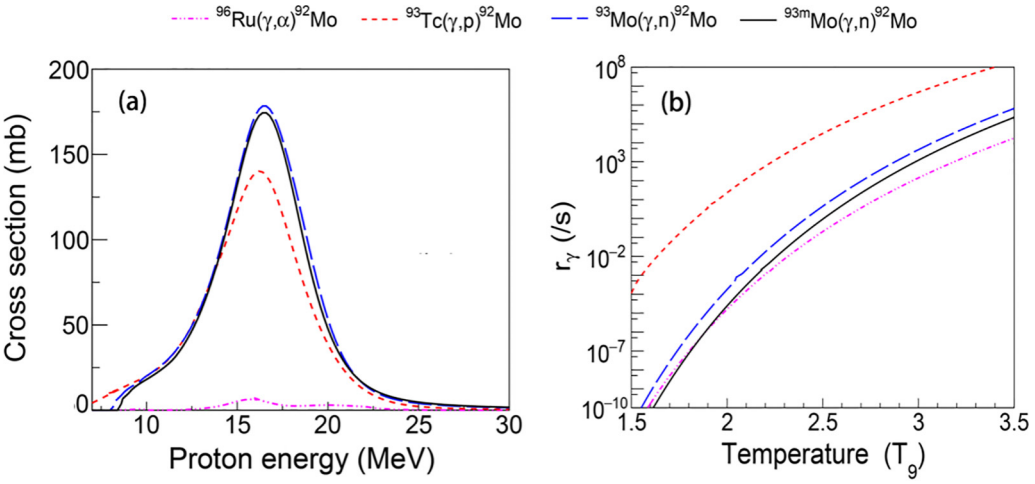

FIG. 8. (a) Cross-section curves of ^{96}Ru(γ, α), ^{93}Tc(γ, p), ^{93}Mo(γ, n), and ^{93m}Mo(γ,n) reactions leading to ^{92}Mo production. (b) Astrophysical reaction rates of ^{96}Ru(γ, α), ^{93}Tc(γ, p), ^{93}Mo(γ, n), and ^{93m}Mo(γ,n) as functions of astrophysical temperature T_9.

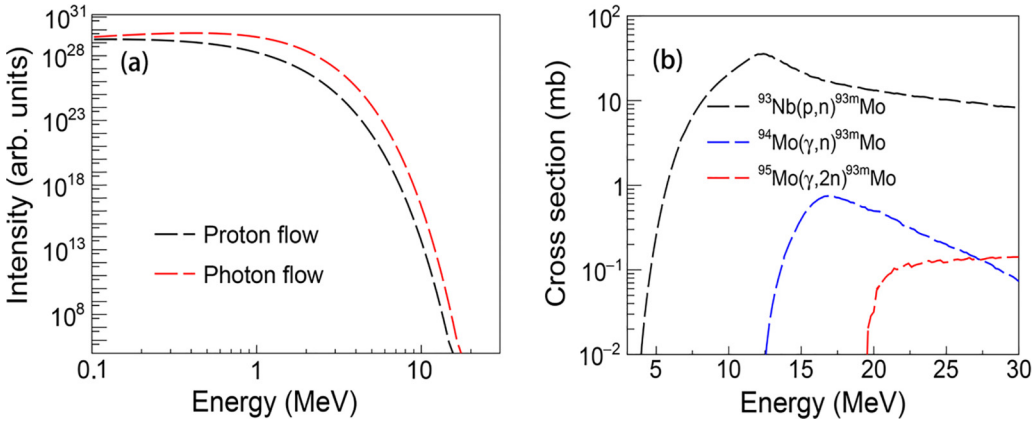

FIG. 9. (a) Spectral patterns of protons and photon flows at the astrophysical temperature of $T_9 = 3.0$. The proton pattern is calculated with Eq. (1) and the photon pattern is considered as the Planck spectrum. To realize the same level of particle flow intensity at the energy of 0.1 MeV, the proton flow intensity is enhanced artificially by a factor of 1.13×10^{35}. (b) Cross-section curves of ^{93}Nb(p, n), ^{94}Mo(γ, n), and ^{95}Mo $(\gamma, 2n)$ reactions leading to ^{93m}Mo production.

comparable with the rates of ^{93}Mo(γ, n) ^{92}Mo and $^{96}(\gamma, \alpha)$Ru ^{92}Mo reactions. This suggests that ^{93m}Mo(γ, n) ^{92}Mo should be considered an alternative nuclear reaction path for ^{92}Mo production at high temperatures of astrophysical interest.

The seed nucleus ^{93m}Mo to produce ^{92}Mo can be synthesized from ^{94}Mo(γ, n), ^{95}Mo $(\gamma, 2n)$, and ^{93}Nb(p, n) reactions. Figure 9(a) shows the spectral distributions of proton and photon flows at the p-process relevant temperature of $T_9 = 3.0$. For these partides, their flow intensities show a flat distribution within the energy range of 0.1–1.0 MeV and then decrease rapidly at higher energies. The comparison between the cross-sections of ^{94}Mo(γ, n), ^{95}Mo $(\gamma, 2n)$, and ^{93}Nb(p, n) reactions are further presented in Fig. 9(b). The maximum cross-section of ^{93}Nb(p, n) ^{93m}Mo is one order of magnitude higher than those of ^{94}Mo(γ, n) ^{93}m Mo and ^{95}Mo$(\gamma, 2n)$ ^{93m}Mo. Meanwhile, ^{93}Nb(p, n) ^{93m}Mo has a visibly lower reaction threshold. Hence, the production of ^{93m}Mo via proton-induced reaction can be sufficient, which may result in a large astrophysical reaction rate. It is expected that the ^{93}Nb(p, n) reaction could play an important role in the production of the seed nucleus ^{93m}Mo, of which the (γ,n) reaction is nonnegligible for the population of the debated p-nucleus ^{92}Mo.

IV. DISCUSSION

In nuclear astrophysics, the astrophysical reaction rate is generally defined as the number of nuclear reactions occurring per unit of time [53]. In this paper, we restrict ourselves to consider the two-body interaction between two nuclei. Since the spectral distributions of the particle flow in astrophysical plasmas can be approximated to the M-B function, the proton-induced astrophysical rate follows [54]:

$$r_p = \sqrt{\frac{8}{\pi\mu}}\left(\frac{1}{KT}\right)^{3/2}\int_0^\infty \sigma(E)E\exp\left(-\frac{E}{kT}\right)dE, \qquad (6)$$

where T_p symbolizes the proton temperature, $\sigma(E)$ denotes the reaction cross-section, and μ is defined as $A_1A_2/(A_1 + A_2)$ with A_1 and A_2 being the mass numbers of the two nuclei involved in the two-body reaction. In our cases, the laser-accelerated proton spectrum resulting from TNSA follows the M-B distribution, which agrees with the one predicted in astrophysical environments. Substituting Eq. (3) into Eq. (6), the astrophysical reaction rate r_p can be directly correlated to the production yield Y:

$$r_p = \sqrt{\frac{8KT}{\pi\mu}}\frac{1}{ndN_p}Y. \qquad (7)$$

This indicates that the astrophysical reaction rate can be obtained by the energy spectrum of the laser-accelerated proton beam when its spectral pattern matches well with the single M-B distribution. However, in the current experiment, the astrophysical reaction rate cannot be derived directly from the spectrum. This is because the present spectrum of the laser-accelerated proton beam is constituted of the M-B distribution with two temperatures, as discussed above. These temperatures are higher than the typical temperature for p-process nucleosynthesis (0.22–0.30 MeV). Nevertheless, it is promising that laser-plasma experiments can be performed to obtain a proton beam with a single M-B distribution at temperatures of astrophysical interest.

V. CONCLUSIONS

We have demonstrated experimentally that ^{93m}Mo isomers are efficiently populated by a laser-accelerated proton beam with a large charge through (p, n) reaction. The production yield of ^{93m}Mo reaches 1.8×10^6 particles/shot, and the resulting peak excitation efficiency is expected to be $> 10^{17}$ particles/s, which is at least five orders of magnitude higher than that of the classical accelerator. This highly efficient excitation of nuclear isomers within the picosecond production time is very useful for the study of isomer depletion processes including NEET and NEEC. We further propose to directly derive the astrophysical reaction rates by using a laser-accelerated proton beam, given that the latter conforms closely to the M-B distribution. Moreover,

the effects of population and destruction of the ^{93m}Mo isomer on the debated *p*-nuclide ^{92}Mo are studied. It is found that the influence of the reaction flow from ^{93m}Mo to ^{92}Mo cannot be ignored, and the ^{93}Nb(p,n) ^{93m}Mo reaction is an alternative route for the production of the seed nucleus ^{93m}Mo. We conclude that the laser-induced proton beam could open an avenue for the production of nuclear isomers with high peak efficiency toward understanding the origin of *p*-nuclei.

ACKNOWLEDGMENTS

We would like to express our thanks to the XingGuang III operation team for their great support. This paper was supported by the National Key R&D Program of China (Grant No. 2022YFA1603300), the National Natural Science Foundation of China (Grant No. U2230133), the Independent Research Project of the Key Laboratory of Plasma Physics, CAEP (Grant No. JCKYS2021212009), the Open Fund of the Key Laboratory of Nuclear Data, CIAE (Grant No. JCKY2022201C152), the Hunan Provincial Natural Science Foundation of China (No. 2023JJ40525), the Research Foundation of Education Bureau of Hunan Province of China (No. 22B0453), and the Hengyang Municipal Science and Technology Project (No. 202150054076).

W.L., Y.Y., and W.Z. conceived and supervised the study. W.F., Y.G., Z.D., Z.Z., and C.T. performed the experiments and analyzed the experimental data. W.F., J.Z., and Z.C. performed the numerical simulations. W.F., W.Q., Y.Y., H.L., X.L., and Y.X. discussed the physics and wrote the paper.

The authors declare no competing interest.

[1] G. Wendell Misch, T. M. Sprouse, and M. R. Mumpower, Astromers in the radioactive decay of *r*-process nuclei, Astrophys. J. Lett. **913**, L2 (2021).

[2] G. Wendell Misch, S. K. Ghorui, P. Banerjee, Y. Sun, and M. R. Mumpower, Astromers: Nuclear isomers in astrophysics, Astrophys. J. Suppl. Ser. **252**, 2 (2021).

[3] C. Fu, G. Zhang, and Y. Ma, New opportunities for nuclear and atomic physics on the femto- to nanometer scale with ultra-high-intensity lasers, Matter Radiat. Extremes **7**, 024201 (2022).

[4] Z. G. Ma, C. Fu, W. He, and Y. Ma, Manipulation of nuclear isomers with lasers: Mechanisms and prospects, Sci. Bull. **67**, 1526 (2022).

[5] Z. H. Xu, Z. Jin, X. Tang, Y. Liu, X. Guo, C. Peng, and H. Wang, Designing performance enhanced nuclear battery based on the Cd-109 radioactive source, Int. J. Energy Res. **44**, 508 (2020).

[6] M. A. Prelas, C. L. Weaver, M. L. Watermann, E. D. Lukosi, R. J. Schott, and D. A. Wisniewski, A review of nuclear batteries, Prog. Nucl. Energy **75**, 117 (2014).

[7] B. Ulmen, P. D. Desai, S. Moghaddam, G. H. Miley, and R. I. Masel, Development of diode junction nuclear battery using ^{63}Ni, J. Radioanal Nucl. Chem. **282**, 601 (2009).

[8] L. Filippi, A. Chiaravalloti, O. Schillaci, R. Cianni, and O. Bagnia, Theranostic approaches in nuclear medicine: Current status and future prospects, Expert Rev. Med. Devices **17**, 331 (2020).

[9] L. Lindenberg, P. Choyke, and W. Dahut, Prostate cancer imaging with novel PET tracers, Curr. Urol. Rep. **17**, 18 (2016).

[10] Z. Cao, W. Qi, H. Lan, B. Cui, X. Zhang, Z. Deng, Z. Zhang, G. Wang, L. Zhang, X. Li *et al.*, Experimental study of medical isotopes ^{62,64}Cu and ^{68}Ga production using intense picosecond laser pulse, Plasma Phys. Controlled Fusion **65**, 055007 (2023).

[11] T. Masuda, A. Yoshimi, A. Fujieda, H. Fujimoto, H. Haba, H. Hara, T. Hiraki, H. Kaino, Y. Kasamatsu, S. Kitao *et al.*, X-ray pumping of the ^{229}Th nuclear clock isomer, Nature (London) **573**, 238 (2019).

[12] B. Seiferle, L. von der Wense, P. V. Bilous, I. Amersdorffer, C. Lemell, F. Libisch, S. Stellmer, T. Schumm, C. E. Düllmann, A. Pálffy *et al.*, Energy of the ^{229}Th nuclear clock transition, Nature (London) **573**, 243 (2019).

[13] L. A. Rivlin and A. A. Zadernovsky, Nuclear gamma-ray laser: A comparative analysis of various schemes, Laser Phys. **20**, 971 (2010).

[14] M. Sadeghi, M. Enferadi, H. Nadi, and C. Tenreiro, A novel method for the cyclotron production no-carrier-added ^{93m}Mo for nuclear medicine, J. Radioanal. Nucl. Chem. **286**, 141 (2010).

[15] Y. Wu, J. Gunst, C. H. Keitel, and A. Pálffy, Tailoring laser-generated plasmas for efficient nuclear excitation by electron capture, Phys. Rev. Lett. **120**, 052504 (2018).

[16] M. Polasik, K. Slabkowska, J. J. Carroll, C. J. Chiara, L. Syrocki, E. Weder, and J. Rzadkiewicz, Resonance conditions for ^{93m}Mo isomer depletion via nuclear excitation by electron capture in a beam-based scenario, Phys. Rev. C **95**, 034312 (2017).

[17] J. Gunst, Y. Wu, C. H. Keitel, and A. Pálffy, Nuclear excitation by electron capture in optical-laser-generated plasmas, Phys. Rev. E **97**, 063205 (2018).

[18] J. Gunst, Y. A. Litvinov, C. H. Keitel, and A. Pálffy, Dominant secondary nuclear photoexcitation with the x-ray free-electron laser, Phys. Rev. Lett. **112**, 082501 (2014).

[19] Y. Wu, C. H. Keitel, and A. Pálffy, ^{93m}Mo isomer depletion via beam-based nuclear excitation by electron capture, Phys. Rev. Lett. **122**, 212501 (2019).

[20] S. Guo, B. Ding, X. H. Zhou, Y. B. Wu, J. G. Wang, S. W. Xu, Y. D. Fang, C. M. Petrache, E. A. Lawrie, Y. H. Qiang *et al.*, Probing ^{93m}Mo isomer depletion with an isomer beam, Phys. Rev. Lett. **128**, 242502 (2022).

[21] D. L. Lambert, The *p*-nuclei: Abundances and origins, Astron. Astrophys. Rev. **3**, 201 (1992).

[22] K. Göbel, J. Glorius, A. Koloczek, M. Pignatari, R. Reifarth, R. Schach, and K. Sonnabend, Nucleosynthesis simulations for the production of the *p*-nuclei ^{92}Mo and ^{94}Mo in a supernova type II model, EPJ Web Conf. **93**, 03006 (2015).

[23] T. Rauscher, G. G. Kiss, G. Gyürky, A. Simon, Z. Fulop, and E. Somorjai, Suppression of the stellar enhancement factor and the reaction ^{85}Rb(p,n) ^{85}Sr, Phys. Rev. C **80**, 035801 (2009).

[24] F. Tárkányi, F. Ditrói, A. Hermanne, S. Takács, and A. V. Ignatyuk, Investigation of activation cross-sections of proton induced nuclear reactions on ^{nat}Mo up to 40 MeV: New data

and evaluation, Nucl. Instrum. Methods Phys. Res. B **280**, 45 (2012).

[25] I. A. Rizvi, K. Kumar, T. Ahmad, A. Agarwal, and A. K. Chaubey, Energy dependence of pre-equilibrium emission for the (p, xn) reactions in niobium, Indian J. Phys. **86**, 913 (2012).

[26] D. Nayak and S. Lahiri, Production of ^{93m}Mo through ^{nat}Y(^{7}Li, $3n$) reaction and subsequent studies on separation and extraction behaviour of no-carrier-added ^{93m}Mo from an yttrium target, Appl. Radiat. Isot. **66**, 1793 (2008).

[27] F. Ditrói, S. Takács, F. Tárkányi, M. Baba, E. Corniani, and Y. N. Shubin, Study of proton induced reactions on niobium targets up to 70 MeV, Nucl. Instrum. Methods Phys. Res. B **266**, 5087 (2008).

[28] S. Guo, Y. Fang, X. Zhou, and C. M. Petrache, Possible overestimation of isomer depletion due to contamination, Nature (London) **594**, E1 (2021).

[29] D. Strickland and G. Mourou, Compression of amplified chirped optical pulses, Opt. Commun. **55**, 447 (1985).

[30] M. M. Günther, O. N. Rosmej, P. Tavana, M. Gyrdymov, A. Skobliakov, A. Kantsyrev, S. Zähter, N. G. Borisenko, A. Pukhov, and N. E. Andreev, Forward-looking insights in laser-generated ultra-intense γ-ray and neutron sources for nuclear application and science, Nat. Commun. **13**, 170 (2022).

[31] W. Qi, X. Zhang, B. Zhang, S. He, F. Zhang, B. Cui, M. Yu, Z. Dai, X. Peng, and Y. Gu, Enhanced photoneutron production by intense picoseconds laser interacting with gas-solid hybrid targets, Phys. Plasmas **26**, 043103 (2019).

[32] Z. G. Ma, H. Y. Lan, W. Y. Liu, S. D. Wu, Y. Xu, Z. C. Zhu, and W. Luo, Photonuclear production of medical isotopes ^{62,64}Cu using intense laser-plasma electron source, Matter Radiat. Extremes **4**, 064401 (2019).

[33] W. P. Wang, C. Jiang, H. Dong, X. M. Lu, J. F. Li, R. J. Xu, Y. J. Sun, L. H. Yu, Z. Guo, X. Y. Liang *et al.*, Hollow plasma acceleration driven by a relativistic reflected hollow laser, Phys. Rev. Lett. **125**, 034801 (2020).

[34] H. Y. Lan, D. Wu, J.-X. Liu, J.-Y. Zhang, H.-G. Lu, J.-F. Lv, X.-Z. Wu, W. Luo, and X.-Q. Yan, Photonuclear production of nuclear isomers using bremsstrahlung induced by laser-wakefield electrons, Nucl. Sci. Tech. **34**, 74 (2023).

[35] J. Feng, W. Wang, C. Fu, L. Chen, J. Tan, Y. Li, J. Wang, Y. Li, G. Zhang, Y. Ma *et al.*, Femtosecond pumping of nuclear isomeric states by the Coulomb collision of ions with quivering electrons, Phys. Rev. Lett. **128**, 052501 (2022).

[36] P. McKenna, F. Lindau, O. Lundh, D. Neely, A. Persson, and C.-G. Wahlström, High-intensity laser-driven proton acceleration: Influence of pulse contrast, Phil. Trans. R. Soc. A **364**, 711 (2006).

[37] S. Agostinelli, J. Allison, K. Amako, J. Apostolakis, H. Araujo, P. Arce, M. Asai, D. Axen, S. Banerjee, G. Barrand *et al.*, GEANT4—A simulation toolkit, Nucl. Instrum. Methods Phys. Res. A **506**, 250 (2003).

[38] W. Luo, H. Y. Lan, Y. Xu, and D. L. Balabanski, Implementation of the n-body Monte-Carlo event generator into the GEANT4 toolkit for photonuclear studies, Nucl. Instrum. Methods Phys. Res. A **849**, 49 (2017).

[39] A. Koning, D. Rochman, J.-C. Sublet, N. Dzysiuk, M. Fleming, and S. van der Marck, Nuclear Data Sheets **155**, 1 (2019).

[40] H. Y. Lan, W. Luo, Y. Xu, D. L. Balabanski, G. L. Guardo, M. La. Cognata, D. Lattuada, C. Matei, R. G. Pizzone, T. Rauscher *et al.* Feasibility of studying astrophysically important charged-particle emission with the variable energy γ -ray system at the Extreme Light Infrastructure–Nuclear Physics facility, Phys. Rev. C **105**, 044618 (2022).

[41] B. A. Remington, R. P. Drake, and D. D. Ryutov, Experimental astrophysics with high power lasers and Z pinches, Rev. Mod. Phys. **78**, 755 (2006).

[42] K. W. D. Ledingham, P. McKenna, and R. P. Singhal, Applications for nuclear phenomena generated by ultra-intense lasers, Science **300**, 1107 (2003).

[43] K. Nemoto, A. Maksimchuk, S. Banerjee, K. Flippo, G. Mourou, D. Umstadter, and V. Yu. Bychenkov, Laser-triggered ion acceleration and table top isotope production, Appl. Phys. Lett. **78**, 595 (2001).

[44] M. Roth, T. E. Cowan, M. H. Key, S. P. Hatchett, C. Brown, W. Fountain, J. Johnson, D. M. Pennington, R. A. Snavely, S. C. Wilks *et al.*, Fast ignition by intense laser-accelerated proton beams, Phys. Rev. Lett. **86**, 436 (2001).

[45] S. C. Wilks, A. B. Langdon, T. E. Cowan, M. Roth, M. Singh, S. Hatchett, M. H. Key, D. Pennington, A. MacKinnon, and R. A. Snavely, Energetic proton generation in ultra-intense laser-solid interactions, Phys. Plasmas **8**, 542 (2001).

[46] G. Martín-Hernández, P. F. Mastinu, J. Praena, N. Dzysiuk, R. Capote Noy, and M. Pignatari, Temperature-tuned Maxwell-Boltzmann neutron spectra for kT ranging from 30 up to 50 keV for nuclear astrophysics studies, Appl. Radiat. Isot. **70**, 1583 (2012).

[47] National Nuclear Data Center. NuDat 3.0, https://www.nndc.bnl.gov/nudat3/.

[48] B. Lawriniang, R. Ghosh, S. Badwar, V. Vansola, Y. Santhi Sheela, S. V. Suryanarayana, H. Naik, Y. P. Naik, and B. Jyrwa, Measurement of cross-sections for the ^{93}Nb(p, n) ^{93m}Mo and ^{93}Nb(p, pn) ^{92m}Nb reactions up to ∼20 MeV energy, Nucl. Phys. A **973**, 79 (2018).

[49] S. Parashari, S. Mukherjee, B. K. Nayak, R. Makwana, S. V. Suryanarayana, H. Naik, and S. C. Sharma, Excitation functions of the p+^{93}Nb reaction in the energy range 10–22 MeV, Nucl. Phys. A **978**, 160 (2018).

[50] F. Ditrói, A. Hermanne, E. Corniani, S. Takács, F. Tárkányi, J. Csikai, and Y. N. Shubin, Investigation of proton induced reactions on niobium at low and medium energies, Nucl. Instrum. Methods Phys. Res. B **267**, 3364 (2009).

[51] P. Morel, J. M. Daugas, G. Gosselin, V. Méot, and D. Gogny, Nuclear excitation by electronic processes: NEEC and NEET effects, AIP Conf. Proc. **769**, 1085 (2005).

[52] K. Vogt, P. Mohr, M. Babilon, J. Enders, T. Hartmann, C. Hutter, T. Rauscher, S. Volz, and A. Zilges, Measurement of (γ,n) the reaction rates of the nuclides ^{190}Pt, ^{192}Pt, and ^{198}Pt in the astrophysical γ process, Phys. Rev. C **63**, 055802 (2001).

[53] F. M. Nunes, G. Potel, T. Poxon-Pearson, and J. A. Cizewski, Nuclear reactions in astrophysics: A review of useful probes for extracting reaction rates, Annu. Rev. Nucl. Part. Sci. **70**, 147 (2020).

[54] W. A. Fowler, Experimental and theoretical nuclear astrophysics: The quest for the origin of the elements, Mod. Phys. **56**, 149 (1984).